

PAPER

Confirmation and variability of the Allee effect in *Dictyostelium discoideum* cell populations, possible role of chemical signaling within cell clusters

To cite this article: Igor Segota *et al* 2022 *Phys. Biol.* **19** 026002

View the [article online](#) for updates and enhancements.

You may also like

- [Three-dimensional single-particle tracking in live cells: news from the third dimension](#)
A Dupont, M Gorelashvili, V Schüller *et al.*
- [Extracellular and intracellular factors regulating the migration direction of a chemotactic cell in traveling-wave chemotaxis](#)
R Ishiwata and M Iwasa
- [Relevance of intracellular polarity to accuracy of eukaryotic chemotaxis](#)
Tetsuya Hiraiwa, Akihiro Nagamatsu, Naohiro Akuzawa *et al.*



IOP | ebooks™

Bringing together innovative digital publishing with leading authors from the global scientific community.

Start exploring the collection—download the first chapter of every title for free.

Physical Biology



PAPER

Confirmation and variability of the Allee effect in *Dictyostelium discoideum* cell populations, possible role of chemical signaling within cell clusters

RECEIVED
30 May 2021

REVISED
15 September 2021

ACCEPTED FOR PUBLICATION
23 December 2021

PUBLISHED
31 January 2022

Igor Segota , Matthew M Edwards , Arthur Campello , Brendan H Rappazzo , Xiaoning Wang , Ariana Strandburg-Peshkin , Xiao-Qiao Zhou , Archana Rachakonda , Kayvon Daie , Alexander Lussenhop , Sungsu Lee , Kevin Tharratt , Amrish Deshmukh , Elisabeth M Sebesta , Myron Zhang , Sharon Lau , Sarah Bennedsen , Jared Ginsberg , Timothy Campbell , Chenzheng Wang and Carl Franck*

Laboratory of Atomic and Solid State Physics, Cornell University, Ithaca, NY 14853, United States of America

* Author to whom general inquiries can be addressed.

E-mail: cpf1@cornell.edu

Keywords: Allee effect, lag phase, chemical signaling, *Dictyostelium discoideum*

Supplementary material for this article is available [online](#)

Abstract

In studies of the unicellular eukaryote *Dictyostelium discoideum*, many have anecdotally observed that cell dilution below a certain ‘threshold density’ causes cells to undergo a period of slow growth (lag). However, little is documented about the slow growth phase and the reason for different growth dynamics below and above this threshold density. In this paper, we extend and correct our earlier work to report an extensive set of experiments, including the use of new cell counting technology, that set this slow-to-fast growth transition on a much firmer biological basis. We show that dilution below a certain density (around 10^4 cells ml^{-1}) causes cells to grow slower on average and exhibit a large degree of variability: sometimes a sample does not lag at all, while sometimes it takes many moderate density cell cycle times to recover back to fast growth. We perform conditioned media experiments to demonstrate that a chemical signal mediates this endogenous phenomenon. Finally, we argue that while simple models involving fluid transport of signal molecules or cluster-based signaling explain typical behavior, they do not capture the high degree of variability between samples but nevertheless favor an intra-cluster mechanism.

1. Introduction

The Allee effect refers to slow or negative population growth rate at low population densities (‘undercrowding’) [1–3]. The relevance of this effect is emphasized in the conservation of endangered species, risk management of invading species that appear harmless when growing slowly at low densities [4, 5] and growth kinetics of tumor cells [6, 7]. The fact that it affects sparse populations often makes it difficult to detect, such as in population studies of large animals with small sample sizes, or cell cultures where it is difficult to accurately measure very low cell density. Nevertheless, in his classic example,

W C Allee demonstrated that multiple goldfish can better alter their environment to the optimal chemical composition than a single fish [1]. He concluded that more members of the same species may lead to fitness benefits in communities with low population density.

Many cellular organisms also exhibit a phase of slow growth (or ‘lag’) at low cell densities, followed by a phase of faster exponential growth. Examples of species showing this phenomenon include *Escherichia coli* [8], *Tetrahymena thermophila* [9], *Paramecium tetraurelia* [10], and *Dictyostelium discoideum* (*D. discoideum*) [11]. However, the interpretation of these slow-to-fast growth (i.e. proliferation) transitions is

confounded by other factors such as variable temperature, presence of other species in the growth medium or dilution from the stationary phase. The traditional literature regards the lag phase as a period in which isolated cells are somehow adapting to a new environment [12], but still begs the question about the mechanism. Consequently, it is not clear whether this slow-to-fast growth rate shift results from an endogenous density (Allee) effect. In our effort we are inspired by the understanding of the Allee effect due to the cooperative extracellular digestion of sucrose in budding yeast [13].

For *D. discoideum*, the focus of this study, common laboratory guidelines specifically emphasize the role of density for suspension cell culture growth, pointing out that growth at densities above $\approx 10^4$ cells ml^{-1} ensures the absence of the slow lag phase [14]. Meanwhile, at lower densities, the culture 'might go through a lag phase' [14]. We previously argued that this is indeed a purely density (Allee) effect, and hypothesized that it could arise from a contact-mediated (juxtacrine) signaling mechanism in a well-mixed shaken cell culture [15].

Here, we first extensively characterize the slow-to-fast transition in *D. discoideum* amoebae and experimentally test the contact-mediated signaling hypothesis. We present evidence for an Allee effect in *D. discoideum* based on a large set of well-controlled experiments and demonstrate large variation in the length of the lag phase. To achieve much more accurate measurements, we developed a novel experimental method for automated cell counting at high temporal resolution (every 10 min) and at very low densities in suspension cultures, orders of magnitude below the turbidity detection limits of spectrophotometers or plate readers. We tested our contact-mediated signaling hypothesis using variable stir rate experiments and show that its predictions do not qualitatively agree with the observations.

Instead, through conditioned media experiments, we demonstrate that chemical signals mediate the slow-to-fast transitions. Finally, we show that a simple chemical signaling model successfully describes the typical behavior within an ensemble of samples, but that the variability observed across samples favors a signaling within cell clusters (i.e. paracrine) explanation.

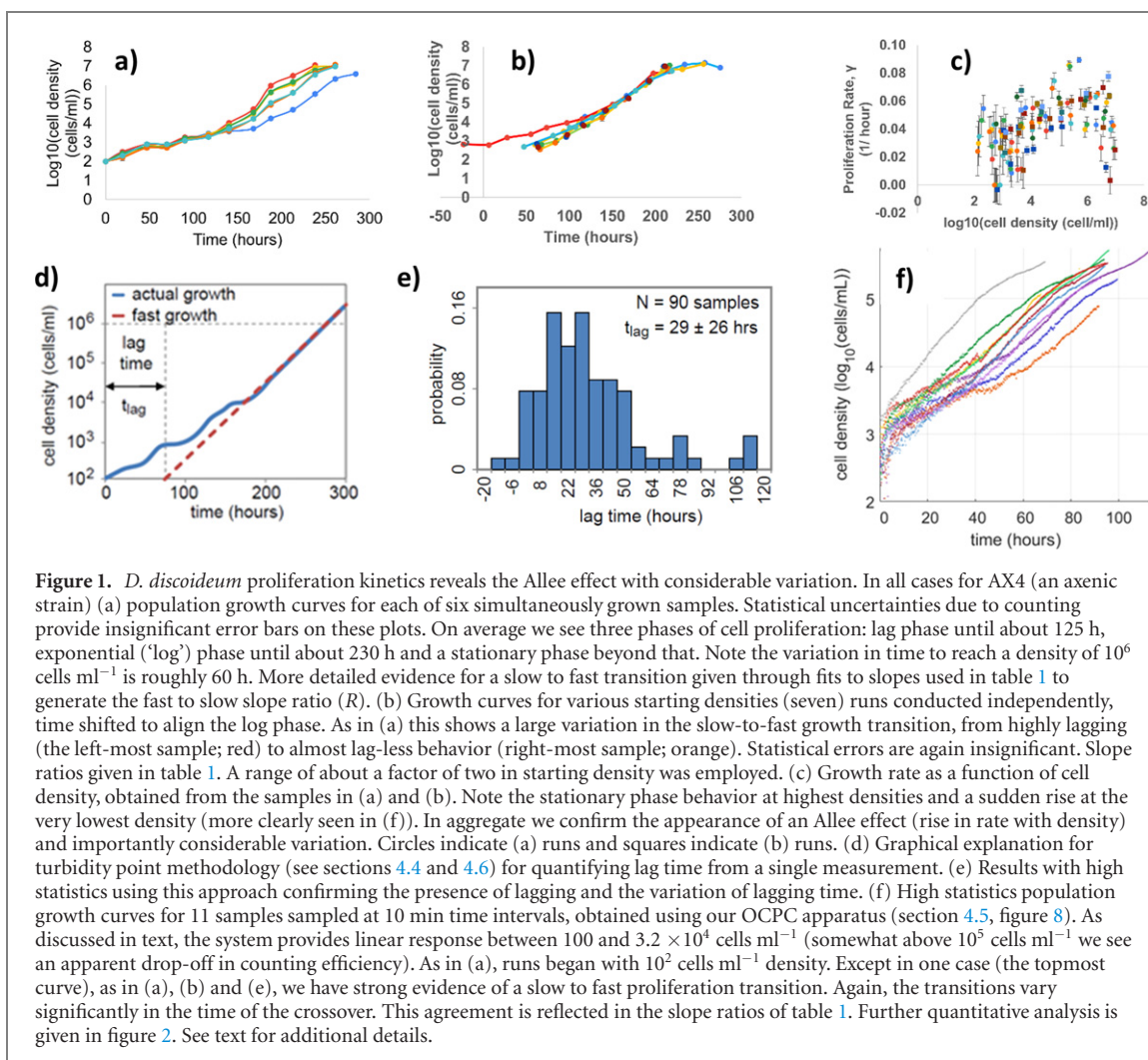
2. Results

2.1. Allee effect shown through population growth measurements

Our first approach to better quantifying the slow-to-fast growth transition in a *D. discoideum* culture is to measure the mean cell density at different times. We sampled cell cultures and counted cells (typically ~ 50 , leading to 15% sampling uncertainty) in a well-defined volume using a hemocytometer; see

section 4.3. We used this method to measure the growth curves (cell density vs time) for samples of the common axenic (i.e. food not provided in the form of another organism, rather as lifeless media) strain AX4. For this experiment, the cells were grown in liquid volumes of 25 ml in shaker culture bottles in the fast growing exponential phase (above 10^4 cells ml^{-1}), and then inoculated at the initial density of 10^2 cells ml^{-1} into fresh culture bottles of equal volume. Figure 1(a) shows the growth kinetics of these runs with the initial data point set to the inoculation density. All the other points have error bars that reflect counting statistics. They are always insignificant in these plots. As we will argue this reveals the slow-to-fast growth transition at a cell density of about 10^4 cells ml^{-1} , about 100 h after inoculation. Typical doubling times obtained by linear regression of log density vs time curves is 18 h for the lag (slow growing) and 11 h for the log (fast growing) phases.

Second, we investigated whether the inoculation density affects the duration of the lag phase. Here, using the same method, we measured the growth curves again for AX4. We ran samples asynchronously and aligned by time translation the growth curves in the fast growing exponential range (from 1×10^4 to 5×10^6 cells ml^{-1}) as shown figure 1(b). While the counting uncertainty again produces barely visible fluctuations in the courses of the proliferation time series, these results show a considerable variation in growth kinetics, from one lagless sample to samples that lag all the way to high densities. Importantly, the starting density which covered a range from 360 to 720 cells ml^{-1} (augmenting the work of figure 1(a) which began with 100 cells ml^{-1}) did not affect the slow-to-fast transition which typically occurred at about 10^4 cells ml^{-1} [see supplemental information (SI) section 1 (<https://stacks.iop.org/PB/19/026002/mmedia>) for additional examples using different inoculant source densities and a second axenic strain]. In table 1 we display and compare for both experiments (figures 1(a) and (b)) R , the ratio of the semilog plot slopes in the log regime over that in the potentially lagging regime (fit details are given in the figure caption). Taking into account statistical counting uncertainty, table 1 shows the same significant run to run variation while confirming the slow to fast transition with time. In figure 1(c) we show that the growth rate $\gamma \equiv \left(\frac{1}{n}\right) \frac{dn}{dt}$ decreases with decreasing cell density n , confirming that we are witnessing an Allee effect at low cell densities. See figure legend for details in all the density regimes. In contrast to the original time series figures 1(a) and (b), here the statistical uncertainty of the numerical differentiation produced considerable uncertainty. Nevertheless, the theme of the persistence of the Allee effect with considerable variation beyond counting statistics is reinforced.



Next, to better quantify this large variation in the lag times, the main observation we focus on in this paper, in our turbidity endpoint technique (section 4.4), we economically performed another type of experiment with 90 smaller samples grown in parallel (0.6 ml each; all with the same initial density of 100 cells ml^{-1}). For this larger number of samples, the cell density was measured only once at high density, between 10^5 and 10^6 cells ml^{-1} , using a turbidity measurement to flag specimens for manual counting. In parallel, control samples inoculated at 5×10^4 cells ml^{-1} were used to establish the exponential phase doubling time. By extrapolating back each exponential growth curve in time, we define the lag time as the time when this extrapolated line crosses the initial density of 100 cells ml^{-1} (figure 1(d)). The measured lag times are presented in figure 1(e). The largest lag times correspond to samples growing in the lag phase with 19 h doubling times up to high densities (e.g., as in the leftmost red sample in figure 1(b)). Small negative lag times are obtained from samples growing slightly faster than controls. We find an aver-

age lag time of 29 h with a standard deviation of 26 h and a broad distribution of at least 60 h. Looking back at the shaker bottle results (figures 1(a) and (b)) we also see a variation in the lag times of at least 60 h.

Finally, to quantify the Allee effect more precisely at a higher temporal resolution and enjoy a tremendous reduction in statistical uncertainty over our previous methods we developed an optical cell passage counting (OCPC) assay. In this device (figure 8, section 4.5) a single, continuously stirred, cell culture is positioned in the path of a green laser beam, with a small illumination volume provided by a low power objective lens. The resulting bright images of cells are relayed through a camera lens and onto a sufficiently fast one-pixel light detector. Each individual cell passing through this volume yields a single light pulse, and the number of pulses is counted in post processing during a fixed amount of time of 10 min. We developed the technique with micron sized colloidal particles, validated the linear response of the system over a wide range of cell densities, and provided an abso-

Table 1. R , ratio of fast to slow regime slopes in figures 1(a), (b), and (f) indicating sizable variation and persistent evidence of a slow to fast transition. For 1(a) and 1(b), the slopes were extracted by weighted (by statistical uncertainties) least squares fit in two regimes: density below 5×10^3 cells ml^{-1} for potential lagging regime (for 1(a) the point at time zero was removed because of the suspected departure from simple exponential growth in the lag phase indicated in figure 1(f)) and above 5×10^4 for the log regime. Data for density beyond 1×10^7 were not fit as this indicate the stationary phase. For the fits to 1(a) and 1(b) the standard deviations in R are given as the uncertainties. For the 1(f) data, by contrast, statistical uncertainties were ignored since they are so small, fits were performed to a pair of straight lines (as indicated in figure 2). See text for more details. In all observations, considerable variation in the transition is shown.

Data set	1(a)	1(b)	1(f)
R values (uncertainties) for each time series	3.0 (0.3)	3.0 (0.4)	1.35 (0.04)
	4.4 (0.7)	1.11 (0.15)	1.84 (0.08)
	2.5 (0.4)	2.7 (1.5)	2.179 (0.015)
	2.3 (0.4)	1.6 (0.5)	No fit
	3.1 (0.3)	1.7 (0.3)	1.90 (0.03)
	3.7 (0.7)	1.67 (0.12)	1.19 (0.06)
		1.68 (0.14)	1.42 (0.04)
			1.32 (0.05)
			1.45 (0.09)
			1.74 (0.05)
			1.24 (0.08)

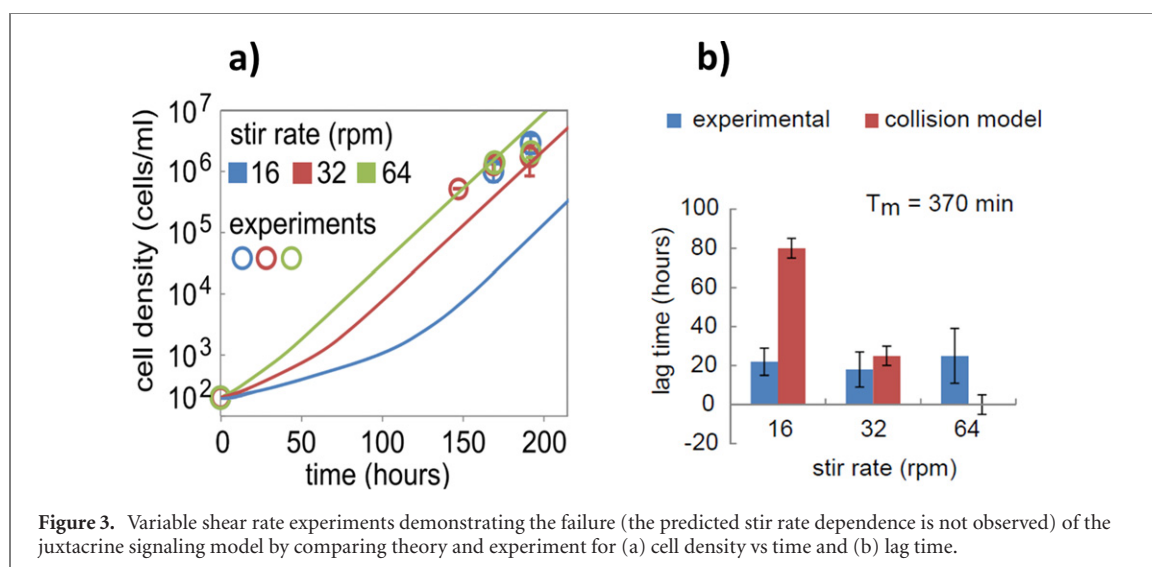
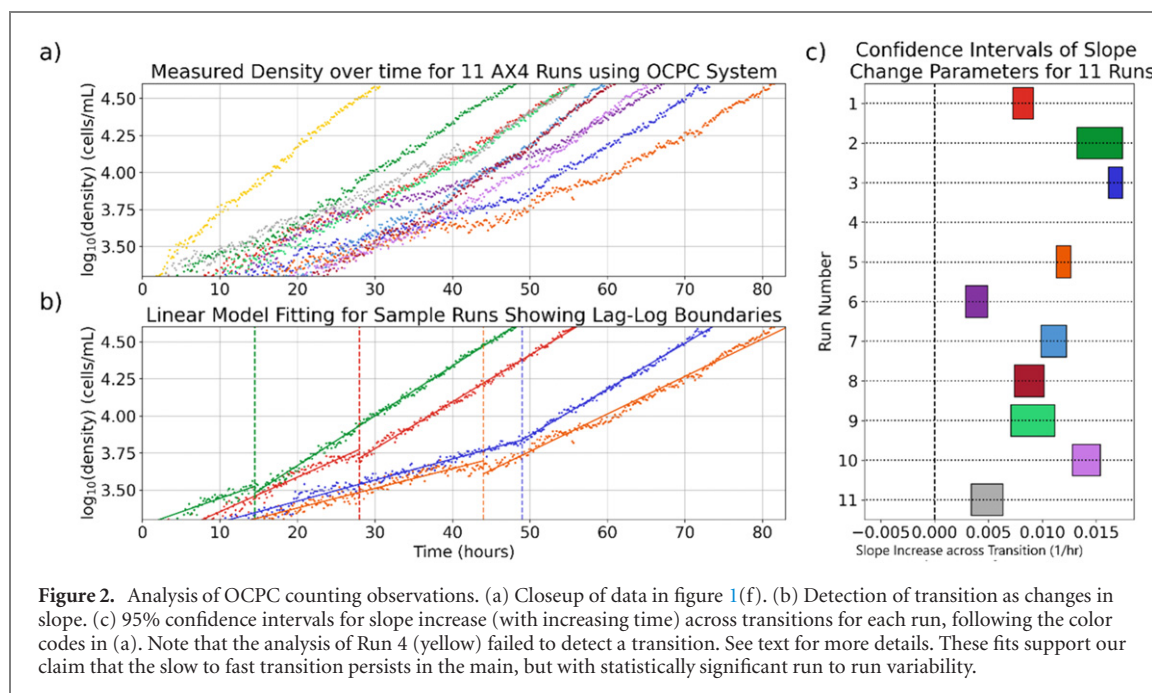
lute calibration. Key to employing this technique was filtering the culture media and performing cell-free medium background measurements. We ran the same experiment 11 times, with AX4 strain cultures starting at 100 cells ml^{-1} . This provided the proliferation time series shown in figure 1(f). We note the expected loss of detection efficiency for cell densities beyond 1×10^5 cells ml^{-1} due to pulse pileup. We see strong qualitative confirmation of our earlier Allee effect observations including variation in lag time: a slow to fast transition cell density of about 6000 cells ml^{-1} , and lag times that covered a range of at least 33 h. In order to bring to bear quantitative statistical uncertainty, we used a different analysis approach than we employed for our shaker culture runs (figures 1(a)–(c)). Since the counting uncertainty is now negligible as shown in the close-up of the putative transition regime in figure 2(a) we checked with linear regression for a linear behavior with a break at a slow–fast transition which the fits delivered as illustrated for a few runs in figure 2(b). Our approach [16] was to maximize the goodness of fit in order to allow the data itself to reveal whether there is a slow to fast transition. As shown in figures 1(f) and 2, this occurred in all but one run. These fits provided changes in slope at the transition as shown in figure 2(c) with increases established within 95% confidence limits. We see that for 10 of the 11 runs the Allee effect is confirmed. In table 1 we show the corresponding R for comparison with the manual shaker culture observation. Through both figure 2 and table 1, we see the earlier pattern of considerable variability in the nature of the Allee effect. At the same time, we discover a new kinetic feature. Figure 1(f) shows an apparent rapid increase in count density at the start of each run. Finally, it is a truly remarkable qualitative result that in contrast to the excess and nonstatistical fluctuations we observe

in the shaker culture manual counting experiments for individual proliferation time series, the great statistical precision afforded by the OCPC assay offers a way to identify the slow–fast transition from run to run not as a broadly defined crossover, but rather as an apparently sharp transition in time.

2.2. Variable stirring rates experiment rules out juxtacrine signaling hypothesis

In earlier work [15], it was argued that cell–cell collisions could have triggered the slow-to-fast transition. This paper developed a contact-mediated (juxtacrine) signaling model where cells divide only after undergoing a critical number of collisions N_C , during a time T_m . This was inspired by apparent evidence that a chemical signal that could be transported by diffusion or fluid flow, i.e. endocrine signaling, was not part of the mechanism behind the transition. A good fit to the data available at the time was provided. Here, we tested the validity of this model by measuring lag times while varying the cell–cell collision rate. We used our turbidity point experiment (see section 4.4), where multiple-vial containers were rotated at different rates (see section 4.6, figure 7).

We used a 32 rpm stir rate experiment to estimate the best-fit values for model parameters as follows: $T_m = 370$ min and $N_C = 1$. The model predicts vastly different lag times for 16 and 64 rpm stir rates, while as shown in figure 3 we observed no change in lag times. In an effort to adapt the model, we found that changing the critical number of collisions N_C to higher values could helpfully extend the predicted lag phase. However, achieving a fit between the experiment and model for larger N_C would require a biologically implausible measurement time T_m , namely larger than the cell doubling time (9–12 h). We concluded that the contact signaling model is not valid.



2.3. Conditioned media effect found but required surprisingly high concentration

Confronted with the failure of the cell collision model, we returned to the notion that cells communicate by means of endocrine signaling. The hypothesis is that cells secrete chemical signals that quickly disperse in a well-mixed suspension and, after reaching a critical concentration, prompt cells to switch to faster growth. To test this possibility, we grew cells in a medium taken from exponentially growing cells [conditioned medium (CM)] and looked for a reduction in the lag time. Previously [15], we did not observe a statistically significant CM effect. In that work we used a small sample number (four) and with only 50% CM diluted in 50% fresh medium. See section 5 of the SI for more details. Having already shown a substantial variation in the population dynamics

at these low densities, we now performed a comprehensive series of CM experiments, with 231 samples run in parallel, using our turbidity endpoint measurement setup (see sections 4.4 and 4.7). This experiment was used to measure lag times for each sample, under a variety of conditions.

We split these samples into three sets, each corresponding to a sub-experiment where we tested the effect of CM prepared from cells at 0.2×10^4 cells ml^{-1} (59 samples), 30×10^4 cells ml^{-1} (120 samples) and 50×10^4 cells ml^{-1} (52 samples), slightly below and above the observed transition density. Conditioning details are given in section 4.7. In each set, we diluted a fraction of CM with our standard growth medium (HL5) into 0% CM (full fresh growth medium), 0.1% CM, 5% CM, and 100% (full CM) fractions. Each sample started with 500 cells ml^{-1} and for each of the three sets and

each of the four CM proportions, we also grew two samples started at 5×10^4 cells ml^{-1} that were used to estimate the fast phase proliferation growth rate. Figure 4 shows the lag time distribution with the CM obtained from specific cell density (column) and diluted by a certain fraction (row).

We observed a statistically significant reduction in the mean lag time between 0% and 100% CM for the 3×10^5 cells ml^{-1} CM and 5×10^5 cells ml^{-1} CM with p -values 2.2×10^{-16} and 5×10^{-3} , respectively (using the Welch two sample t-test; see SI section 8). In addition, we observe progressive reduction in the lag time distribution as the fraction of CM is increased, although we still observe large variation and an occasional big outlier. This conclusively demonstrates that the slow-to-fast growth transition arises from a chemical signal.

Assuming that the putative proliferation factor sustains fast proliferation over the entire density range of the exponential phase, we are surprised that we detected a significant conditioned media effect only for the very highest concentration of conditioned media.

2.4. The variation in the Allee effects is intrinsic

As discussed in sections 1 through 4 of the SI we tested for the importance of different strains and the inoculant source density (which might indicate the importance of previously established proliferation suppression factor), searched for a lagless strain, adapted our cell culture techniques, and tested for possible bacterial contamination. In none of these tests could we find a factor that systematically affected the Allee effect. Our careful cell culture procedures have ruled out the possibility of new lagging/non lagging phenotypes evolving from successive cell culture progressions. We therefore concluded that the observed Allee effect variation is an endogenous behavior. We therefore sought an explanation for the run to run fluctuations in the proliferation kinetics.

2.5. Mechanisms for variation of the cell proliferation kinetics and the Allee effect without invoking intercellular interactions ruled out

In sections 6 and 7 of the SI, we respectively eliminate the possibilities that the natural variations in the cell cycle and fluctuations in the initial inoculation of samples are responsible for the observed variation in growth proliferation time series. In neither case do these approaches offer an explanation for the observed Allee effect. We therefore turn to models besides our now-discarded juxtacrine signaling approach that include intercellular interactions to understand the observed Allee effect and its variation.

2.6. Endocrine and cluster-based models can explain the average lagging behavior but differ on the degree of variation of lag time

Endocrine model. Given our observation that conditioned media affects the distribution of lag times, we first provide a simple endocrine signaling model. We model cells as growing at a rate γ_{slow} until a critical number of signaling receptors R_c (out of R_T total receptors) are occupied on each cell, at which point each cell irreversibly switches to a fast proliferation growth rate γ_{fast} (figure 5(a)). Both cell types produce a growth factor c at a rate v per cell. The dynamical equations for the densities of slow-growing cells n_s , fast-growing cells n_f and growth factor concentration c are (ignoring the stationary phase):

$$\frac{dn_s}{dt} = \gamma_s n_s - W_{s \rightarrow f} n_s \quad (1)$$

$$\frac{dn_f}{dt} = \gamma_f n_f + W_{s \rightarrow f} n_s \quad (2)$$

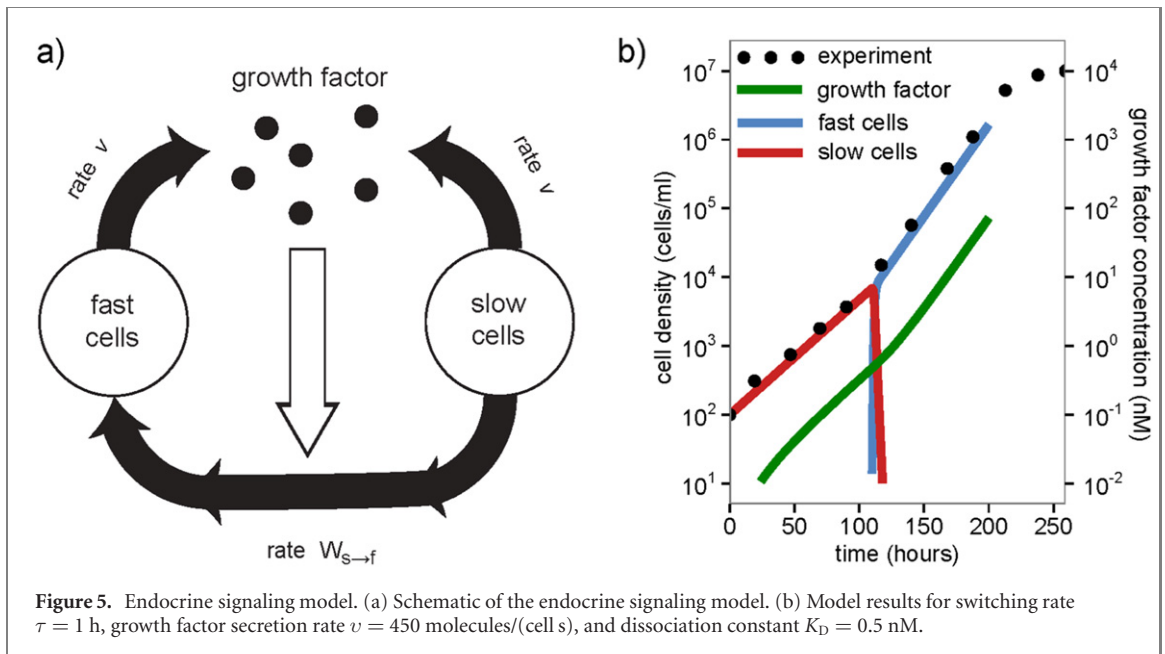
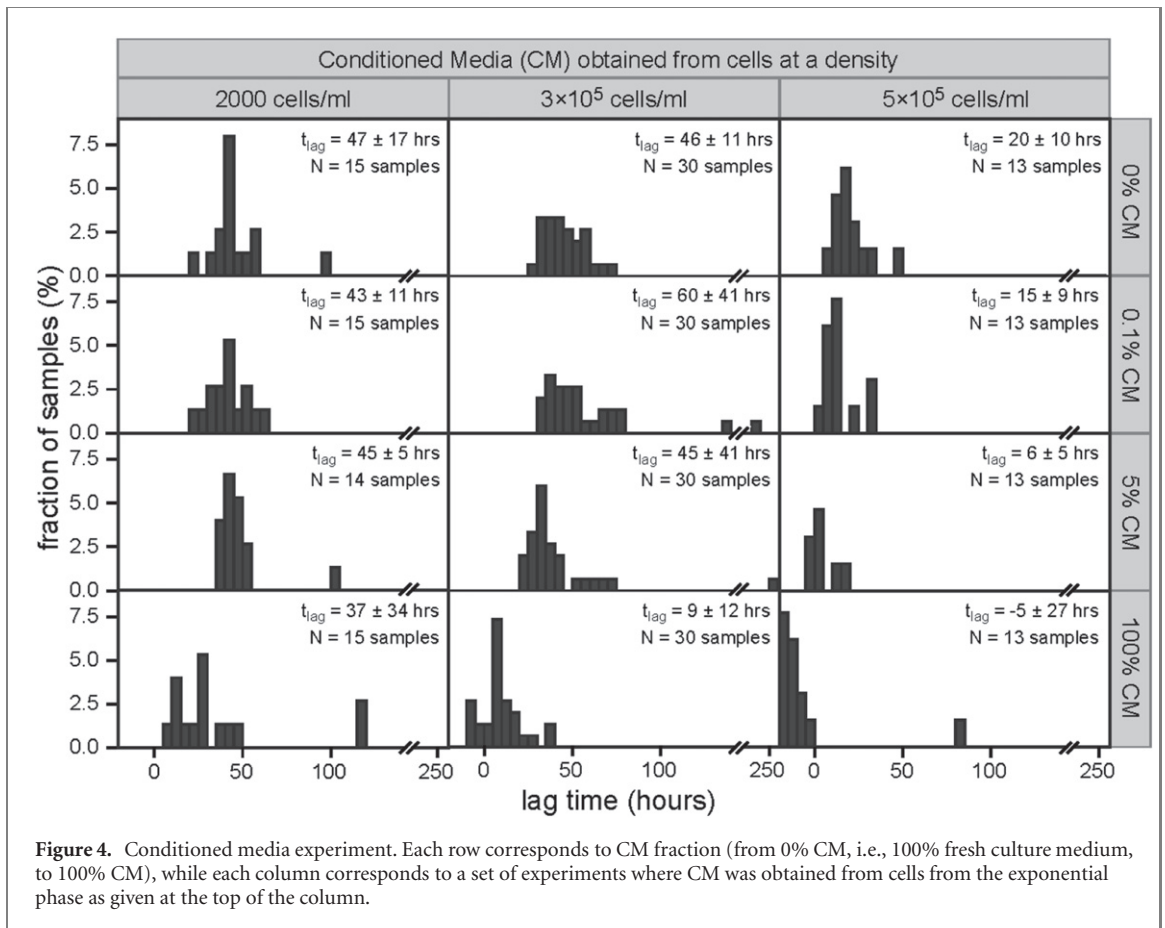
$$\frac{dc}{dt} = v (n_s + n_f). \quad (3)$$

In the above, $W_{s \rightarrow f}$ is the rate of conversion from slow to fast growth per cell. $W_{s \rightarrow f}$ is given by the product of the characteristic transition rate $1/\tau$ and the fraction of slow growing cells that have R_c or more occupied receptors, which follows a binomial distribution:

$$W_{s \rightarrow f} = \frac{1}{\tau} \sum_{R=R_c}^{R_T} \binom{R_T}{R} \left[\frac{c(t)}{c(t) + K_D} \right]^R \left[\frac{K_D}{c(t) + K_D} \right]^{R_T - R},$$

where $\frac{c(t)}{c(t) + K_D}$ is the probability of a single receptor being occupied in chemical equilibrium with the external signal at concentration $c(t)$ and having a dissociation constant K_D . We take $R_T = 10\,000$ receptors per cell from reference [17] page 30 and estimate that $R_c = R_T/2$. Rough estimates (see SI section 9) show v is typically in the range 400–9000 molecules/(cell s). Since only the total cell number density was measured here ($n_s + n_f$), the results of this model depend on v and K_D through the combination v/K_D . For the range of dissociation constants for growth factors $0.08 \text{ pM} \leq K_D \leq 20 \text{ nM}$, typically around 0.5 nM [17], the value for v that fits the data is 450 molecules/(cell s), consistent with biologically meaningful estimates. Changing the conversion time τ does not affect the model fit (up to 25 h), but only changes the time scale at which fast growing cells take over the population, making the transition smoother. In summary, an endocrine signaling model can describe the typical [18] time series behavior of the slow-to-fast growth transition as shown in figure 5(b).

Let us now consider the expected variation in the cell density growth curves due to chemical binding fluctuations in the signaling event in this mechanism.



From reference [17], p 141, the variation in the probability of occupancy of a receptor (θ) is given as follows:

$$\sigma_{\theta}^2 = \frac{cK_D}{R_T(K_D+c)^2}.$$

While the average value of θ is given by: $\frac{c}{K_D+c}$.

How do these fluctuations affect the value of c at the transition, $c_x = K_D$?

By differentiation of the above we discover:

$$\sigma_{c_x} = \frac{2K_D}{R_T^{1/2}}.$$

This in turn provides (see SI section 9) the fluctuation in the expected crossover cell density through

the relation: $c_x = \frac{v}{\gamma_{slow}} n_x$.
This gives us: $\frac{\sigma_{n_x}}{n_x} = \frac{2}{R_T^{1/2}}$.

From reference [17], p 30 we have $R_T = 900$ to 7×10^5 receptors/cell (typically 3×10^4 for epidermal growth factor). We therefore conclude that $\frac{\sigma_{nx}}{n_x} = 0.066$ to 0.0024 (typically 0.012).

Turning to the observed variation in the lag time which we conservatively estimate is at least 10–15 h, (a limit considerably smaller than the observed range) using $\gamma_{\text{slow}} = 0.038 \text{ h}^{-1}$ by fitting the typical lag phase in figure 1(a), that implies an observed range of: $\frac{\sigma_{nx}}{n_x}$ of at least 0.4 to 0.6. This is considerably greater than the theoretical estimate given above. Relaxing the requirement that $c_x = K_D$ means that: $\frac{c_x}{K_D} < 6.9 \times 10^{-3}$ or > 145 . Either option seems implausible given that we expect $c_x \approx K_D$. We do note however that in earlier work on folic axis chemotaxis [19], we observe that response can occur even at $\frac{c}{K_D} \approx 100$. We conclude that the variation in proliferation time series that we notice is unexplained by this simple endocrine model.

Cluster sourced endocrine model. Here, building upon observations of cell aggregation in suspensions [15, 20] we analyze possible growth signaling models based on cell clusters. In contrast to the previous model which could be solved analytically, here we need to perform simulations. We assume that the cells cluster with a rate α , that cells in clusters have a characteristic lifetime τ to remain in a cluster, and that only the cells in clusters produce proliferation growth factors with a rate ν per cell. The equations describing the population dynamics in this model are as follows. Here, n is the density of single cells, n_c is the overall density of cells that belong to clusters, and c is the concentration of growth factor:

$$\begin{aligned} \frac{dn}{dt} &= \underbrace{-\alpha(n+n_c)n}_{\text{clustering}} + \underbrace{\frac{n_c}{\tau}}_{\text{cluster decay}} + \underbrace{\gamma(c)n}_{\text{cell proliferation}} \\ \frac{dn_c}{dt} &= \alpha(n+n_c)n - \frac{n_c}{\tau} + \gamma(c)n_c \\ \frac{dc}{dt} &= \nu n_c. \end{aligned}$$

The growth rate is given empirically, assuming a switch-like cell behavior:

$$\begin{aligned} \gamma(c) &= \gamma_{\text{slow}} \quad \text{if } c < c_x \\ &= \gamma_{\text{fast}} \quad \text{if } c > c_x, \end{aligned}$$

where γ_{slow} and γ_{fast} are estimated by fitting the typical low and high-density slopes of figure 1(a) respectively (see SI section 9 for our estimation of c_x). One can interpret the clustering term as the collision rate of single cells with each other $\sim \alpha n^2$ and the collision rate of isolated cells with clustered cells $\sim \alpha n n_c$. We express the entire model schematically in figure 6(a).

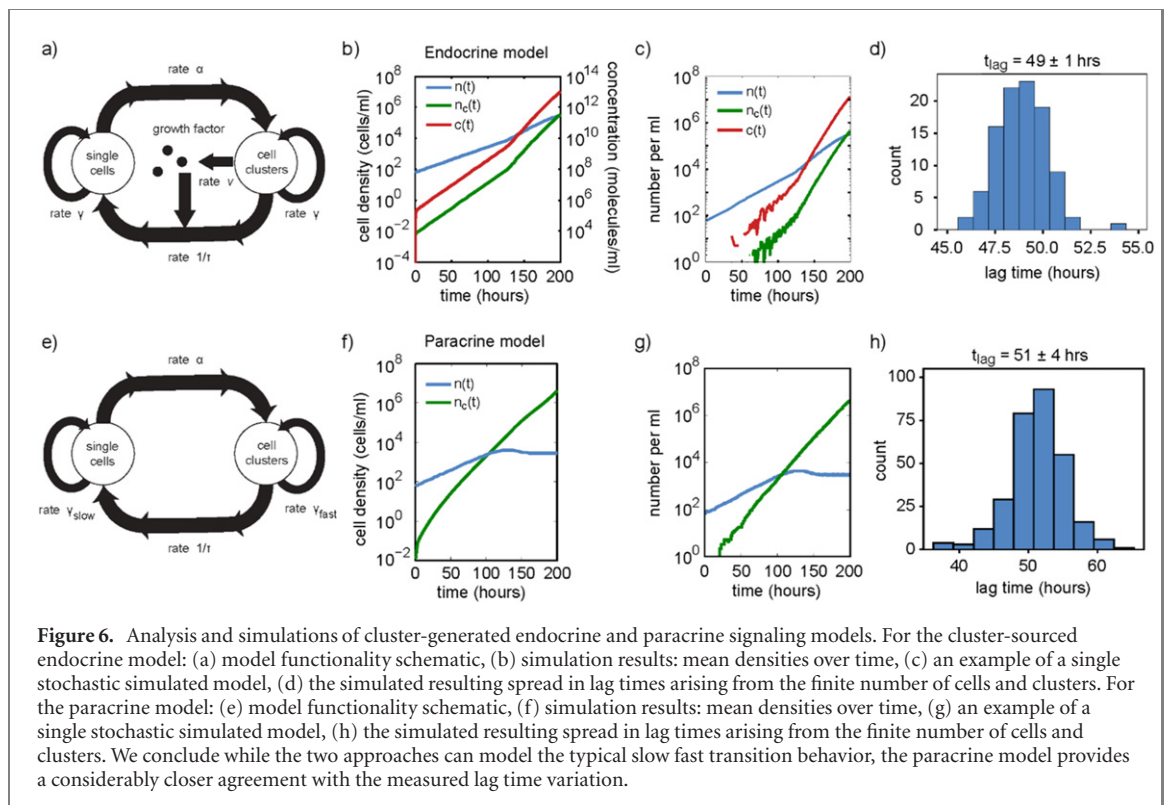
We estimated the clustering rate coefficient α according to the shear-induced flocculation theory of Probstein [21]. We took the cells in suspension to be spheres of 5 micron radii and applied the theory to

our turbidity point studies by estimating the shear rate as $2\pi f$ where f , the vial rotation rate, was taken as 16 rpm. This yielded $\alpha = 10^{-9} \text{ s}^{-1}$. To estimate the cluster decay rate ($1/\tau$) we turned to observations of clusters on glass substrates (see section 4.8). Since we could not monitor these clusters in suspension, we observed the fusion of cells and cell-clusters on substrates and noted their subsequent partial or total breakups. Averaging the time intervals between cluster formations and breakups provided an average cluster lifetime result of $\tau = 30 \text{ min}$. We found that we could fit typical [18] observations of figure 1(a) with growth rates corresponding to doubling times in the lag and log phase of 18.3 and 11.3 h, respectively, if we set the growth factor secretion rate at $\nu = 2000 \text{ molecules}/(\text{cell s})$. This lies well within the estimated range of 400–9000 molecules/(cell s) detailed in SI section 9. Using these parameters, we ran Gillespie simulations in MATLAB[®] (see SI section 10) to predict the stochastic behavior of the cluster-sourced endocrine mechanism in our turbidity point experiment at 16 rpm. Figures 6(b) and (c) show, respectively, the average simulated behavior and the result of a single simulation. While the average results are in good agreement with our observations the resulting variation in lag time of 1 h (as shown in figure 6(d)) is much smaller than that we observed in either the daily cell-counting or turbidity point experiments (shown in figures 1(a), (b) and (e) respectively).

Paracrine model. Finally, we also considered a paracrine signaling, i.e. secretion and detection of a chemical signal between neighboring cells, model (given schematically in figure 6(e) and detailed in SI section 10) where single cells proliferate at a slow rate γ_{slow} and clustered cells grow at a fast rate γ_{fast} , while the clustering dynamics remain unchanged from the previous model:

$$\begin{aligned} \frac{dn}{dt} &= \underbrace{-\alpha(n+n_c)n}_{\text{clustering}} + \underbrace{\frac{n_c}{\tau}}_{\text{cluster decay}} + \underbrace{\gamma_{\text{slow}}n}_{\text{cell proliferation}} \\ \frac{dn_c}{dt} &= \alpha(n+n_c)n - \frac{n_c}{\tau} + \gamma_{\text{fast}}n_c. \end{aligned}$$

We estimated the cell-clustering rate α from the shear induced collision rate ($\alpha = 10^{-9} \text{ s}^{-1}$ as before). The number of clusters n_c and the cluster decay time τ were estimated based on surface growth measurements as before ($\tau = 30 \text{ min}$). We found, again, that we could fit typical [18] experimental observations from figure 1(a) with growth rates corresponding to doubling times in the lag and log phase of 18.3 and 11.3 h, respectively, with a factor secretion rate at $\nu = 2000 \text{ molecules}/(\text{cell s})$. Again, running Gillespie simulations in MATLAB[®] (see SI section 10) of the paracrine mechanism, assuming our turbidity point setup at 16 rpm, as before, we obtained figures 6(f)



and (g). These show, respectively, the average simulated behavior and the result of a single simulation run. The lag time histogram from multiple runs (shown in figure 6(h)) shows a lag time variation of 4 h, significantly smaller than observed but closer to observations than the other models.

Model comparison. A non-cluster-based endocrine signaling approach yields a much lower than observed value for the variation in the lag time. The stochastic Gillespie simulations we performed for both cluster-sourced endocrine signaling and the paracrine signaling give lag time variation of 1 and 4 h, respectively. While cluster-sourced endocrine and the paracrine mechanisms yield estimated lag time variations far lower than those we observed in our experiments, the paracrine signaling approach is decidedly closer to what we observe.

3. Discussion and conclusion

We studied a density-dependent proliferation transition in *D. discoideum* amoeba. Whereas many [22] have investigated the starvation response aggregation of *D. discoideum* at much higher cell densities ($\sim 10^6$ cells ml^{-1}), we focused our attention on a low-density example of the Allee effect displayed by many other single-cellular, plant, and animal species.

We previously offered a collective explanation for a slow-to-fast growth transition based on cells sensing each other's presence through collisions (juxtacrine signaling) [15]. In this current work we apply the observation of clustering on a substrate to the

problem of clustering in a suspension. This qualitatively agrees with other studies of cell–cell adhesion in suspension [20]. Here, through a much more extensive set of experiments than in that earlier work, we rule out the juxtacrine signaling hypothesis and argue that either (i) a cluster-sourced endocrine signaling mechanism serves as a cell density signal through the production and transport of soluble proliferation factors or (ii) more likely communication happens through a paracrine signaling mechanism, where neighboring cells in one cluster exchange growth factors.

The positive result of our conditioned media experiment confirms that a chemical signal mediates these mechanisms. We also show that significant variations in the growth rates at densities below 10^5 cells ml^{-1} are characteristic of this system and not artifacts of low density cell cultures, e.g., the effects of contamination by a rival organism. Uncertainties in inoculation densities, variations due to different positions in the cell cycle, and fluctuations in receptor–ligand binding, do not explain the observed time-variation around the density threshold among different samples. An explanation of the precise variation we observe requires further work, but stochastic simulations demonstrate that of the models we have explored most closely matches that arising from a paracrine signaling model. As an alternative to the generation and distribution of proliferation factors hypothesis mechanism for the Allee effect we are discussing here, Nathalie Balaban [23] has suggested that we might be observing a collective detoxification of the culture medium.

Looking carefully at the OCPC system result of figure 1(f), we note an initial, sudden rise in apparent cell density. It occurs to us that this might reveal the breakup of cell clusters when the bulk log phase source employed is introduced into a dramatically diluted environment. It would be valuable to monitor the size of particles counted, at the very least for this reason but even more importantly as a means of providing a deeper test of the cluster-based models introduced. Additionally, as shown in figure 2, in contrast to the manual counting experiments of figures 1(a) and (b), this same assay opens the door to providing a sharp determination of the point of transition between slow and fast proliferation, a feature to be monitored for evidence of the sources of variation in the Allee effect.

From the perspective of evolutionary biology, an Allee effect might benefit *D. discoideum* cell colonies. The presence of other cells in the environment could indicate abundant nearby nutrients, as the cell density at this point (10^4 cells ml^{-1}) falls under the levels where cells compete for resources and proceed to the stationary phase ($\sim 7 \times 10^6$ cells ml^{-1}). One could investigate this further by coupling our understanding of this effect with current models of biological behavior centered around concepts in game theory [24]. The cellular Allee effect could possibly arise from a set of well-defined initial conditions paired with common strategies across cells in response to an extensive payoff matrix. The construction of such a model would allow more concrete insights into the mechanisms underlying the Allee effect in different natural environments. This would allow researchers to more accurately predict cell growth kinetics given sets of conditions pertaining to specific environments (e.g., early-stage tumor growth in various parts of the human body).

Future work on this investigation can branch into several directions. To begin with, there exists a possibility that memory effects in the slow-to-fast transition allow each state to persist through generations (e.g., a phenotypic switch). This hypothesis would suggest that an epigenetic mechanism could lead to the wide variation in transition times by leaving cells in one (slow growth) state or the other (fast growth). One could run experiments to attempt to select for fast (or slow) growing cells by repeatedly selecting for the fastest (or slowest) growing samples and culturing them through several generations. Also, we have not yet ruled out the possibility of isolating a completely lagging (consistently slow growing) or a lagless (consistently fast growing) strain. Future work in this regard could be enabled by growing monoclonal *D. discoideum* colonies in a batch. This effort could also help estimate the effect of subtle genetic diversity on the observed variation in lag times. Also, we could make more direct observations by studying the slow-to-fast transition on a substrate in two dimensions. Thus far, indications [15, 25] are that cells in such a

system do not lag, but more extensive work is warranted especially with hydrophobic substrates that foil cell adhesion. For example, if the slow growing cells got stuck in a particular phase of the cell cycle, a *D. discoideum* strain with a green fluorescent protein (GFP) marker for that phase [26] could indicate the doubling time for individual cells. In addition, one could easily observe and quantify any possible correlation between the doubling time and the local cell surface density. Also, Bastounis *et al* [27] demonstrated the critical role that the manner of shaking plays in cell division, specifically that non-inertial flow in non-orbital shakers suppresses cytokinesis. Despite our demonstration that proliferation as a function of shear rate does not follow our collision theory for intercellular signaling, subtler variable degrees of mixing preparations may lead to new conclusions. We could further alter the degree of coalescence between cells using tools such as ultrasonic agitation and the infusion of the chemical suppressor of cell–cell adhesion in *D. discoideum*, ethylenediaminetetraacetic acid (EDTA) [20]. Considering the comments of Robert Insall [24], the exploration of other strains can further our understanding of proliferation control mechanisms present in genuinely wild type *D. discoideum* that the axenic strains AX3/4 lack. Thus, one can look forward to the exploration of non-axenic suspension growth strains, where both the density of *D. discoideum* cells and that of a bacterial food source are important. Finally, regarding our modelling, in particular for cluster-based mechanisms for proliferation, we can look forward to going beyond the zero spatial dimensional approach used here to include full three dimensional simulations.

4. Materials and methods

4.1. Use of biological vs technical replicates

In all measurements except for our automated continuous counting assay, our experiments were performed with biological replicates [28] since the essence of our work is that we observe sample to sample variation in our time series. For the automated experiment, the sampling of a given run is rapidly repeated on the time scales shorter than the characteristic times associated with the time evolving features which we observe. Thus while the experiment was performed as all others with biological replicates (eleven in this case), the measurements were technically repeated on short time scale in order to achieve high statistical precision.

4.2. Cell culturing and inoculation

Cell culturing followed a standard shaker protocol [14] with the addition of penicillin and streptomycin (PenStrep; Invitrogen) antibiotics. We define a unit PenStrep dose as one of $25 \mu\text{g ml}^{-1}$ (we thank Petra Fey of Northwestern University's Dicty Stock Center for this suggestion). We define a

unit tetracycline dose as one of $30 \mu\text{g ml}^{-1}$, as used previously in *D. discoideum* as an expression system (as noted by Petra Fey [23]). Closed 100 ml Erlenmeyer flasks containing 25 ml of HL5 culture media [14] treated with 2500 units of penicillin and 2.5 mg of streptomycin ($250 \mu\text{l}$ per 25 ml bottle) were shaken constantly at 150 rpm on an orbital shaker after inoculation from exponentially growing cultures.

4.3. Daily visual cell counting method

We first measured cell densities by visually counting cells in cultures at daily intervals using a hemocytometer—Model 4000 *Nageotte Counting Chamber* (Hausser Scientific, Horsham, PA). This allowed for precise measurements down to $100 \text{ cells ml}^{-1}$. In comparison with cell-free containers of culture media, the false-positive background density corresponded to typically 60 but up to $180 \text{ cells ml}^{-1}$, presumably because of visual misidentification of particles in the media as cells. The statistical counting uncertainties for these experiments (e.g. SI figures S1(a) and (b)) were typically 40% at $100 \text{ cells ml}^{-1}$ and 22% at $1000 \text{ cells ml}^{-1}$ and higher densities. For figures 1(a)–(c) the counting uncertainties were precisely determined from the raw data.

4.4. Turbidity point measurement method

While individual-culture measurement methods like the one described above allow us to measure individual growth curves, culturing many samples and measuring them daily requires a considerable amount of time which limits the sample size. In an alternative setup, we employed many small (1.8 ml) vials each containing 0.6 ml of cell suspension in rotating drums (see figure 7). Each day, we simultaneously measured the turbidity of each vial to determine when the cell density had reached approximately $10^6 \text{ cells ml}^{-1}$. Once the samples became turbid, we measured the cell density precisely using the hemocytometer described in the previous method.

The rotating drum was mounted on a stepping motor shaft. We operated the motor at speeds between a specific range to minimize vibrations since we were interested in performing controlled shear rate experiments (see section 4.6). Running the stepping motor at too low a rate (\sim few rpm) would produce a stepping motion that, in turn, would cause the flow within vials to become jerkily inertial and not viscosity dominated. Running the motor too fast, on the other hand, could introduce mechanical resonances and, again, produce vibrations leading to inertial mixing.

We checked the turbidity of each vial in our drum mixers using a system consisting of a red laser diode and a phototransistor monitor in line with the laser beam (forward scattering). We calibrated the system with samples of well-defined cell densities, checked

using a counting chamber. In the rare case of bacterial infections, the vial would turn very turbid, and we could detect the infection within a day and discard the vial.

In the course of this work, it was discovered that an apparent change in the manufacture (by following lot numbers) of the vial cap liners resulted in a significant increase in the doubling times. This problem which did not affect the data presented here was cured by rinsing with 65% isopropyl alcohol and drying.

4.5. Automated continuous counting method

To obtain more accurate measurements in an automated and continuous way, we developed our own cell density measurement method centered around an OCPC setup (figure 8). In this approach one counts cells in a sampling volume by registering them as flashes of light that pass across a single element detector. Our design involved a green laser diode source—focused with a low-power objective lens—positioned to shine through the center of a continuously stirred 10 ml culture in a 0.75 inch diameter sample cell made from a cut test tube capped with a rubber septum. A magnetic stir bar at the bottom of the chamber was driven by a permanent magnet rotated at 151 rpm (as in our shaker cultures) by a stepping motor. We positioned a light detector downstream from the laser with a lens that imaged in a direction 40 degrees from the forward direction with roughly $0.7\times$ demagnification of a portion of the illuminated sample region on the detector. The photodiode detector had a 5.1 mm^2 active area. A green filter blocked orange fluorescence produced by the culture media. This allowed us to capture a range of cell counts from the lowest densities, through the slow–fast transition, and well into the exponential proliferation regime. We covered these components with a light-shielding box to minimize unwanted noise from room lights.

To count light flashes accurately, we employed a computer running the remarkable pulse height analysis program PRA which was originally intended for gamma ray spectroscopy with energy sensitive detectors [29]. We developed the technique by running the experiment with suspensions of 10 micron-diameter colloidal particles, aimed to mimic cells in shape and size. Employing PRA's 'shape tolerance method', we found an approximate pulse time profile corresponding to a cell which the PRA program could discern from noise.

With an appropriate pulse profile, we could run the experiment on filtered (0.25 micron) media without cells and subtract the resulting pulse height spectrum from that produced by a run with cells to obtain a background-subtracted result. We found that attempting this with the wrong selected pulse width would lead to non-meaningful spectra with negative net 'counts'. We repeated these subtractions with manually adjusted pulse width ranges until

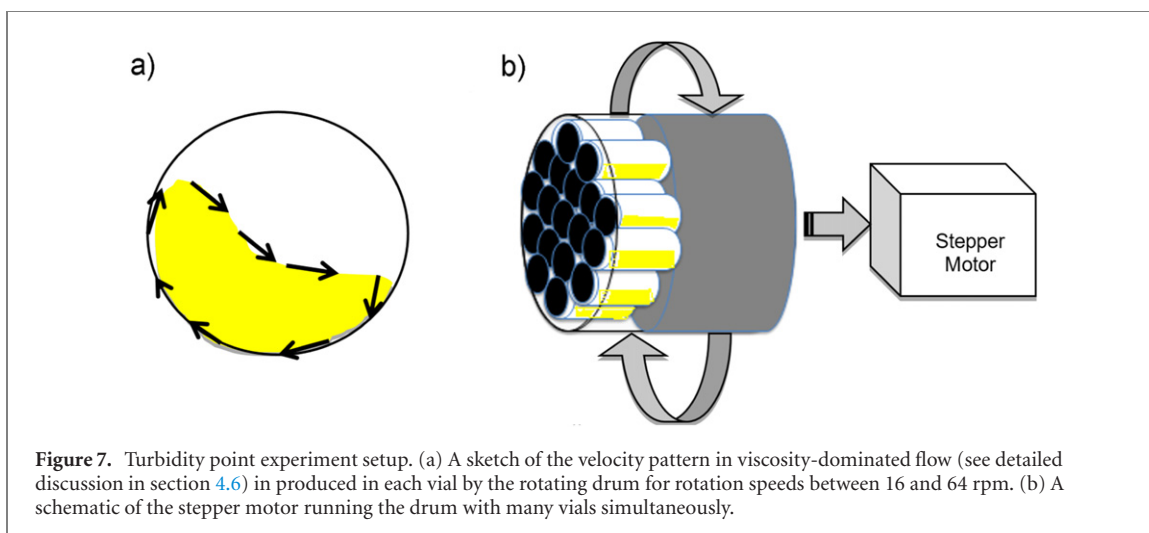


Figure 7. Turbidity point experiment setup. (a) A sketch of the velocity pattern in viscosity-dominated flow (see detailed discussion in section 4.6) in produced in each vial by the rotating drum for rotation speeds between 16 and 64 rpm. (b) A schematic of the stepper motor running the drum with many vials simultaneously.

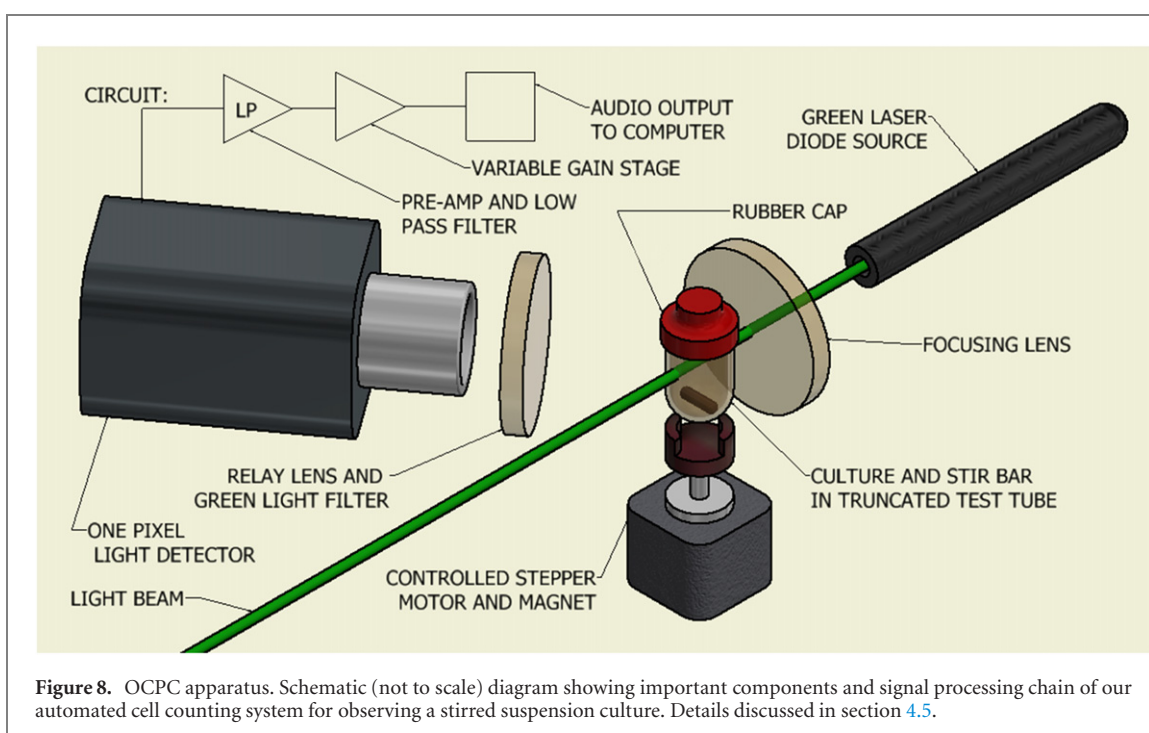


Figure 8. OCPC apparatus. Schematic (not to scale) diagram showing important components and signal processing chain of our automated cell counting system for observing a stirred suspension culture. Details discussed in section 4.5.

we obtained strongly positive, biologically meaningful results. Scrupulous attention was paid to stray sources of dust that would introduce extraneous particle counts [30].

Using these optimization methods, we trained the PRA program to identify cells as efficiently as possible. Our colloid particle detection efficiency exceeds our cell counting efficiency by a factor of 32.

This result allowed us to record the cell density of the culture at ten minute intervals within our density range of interest. As seen in figure 1(f), at approximately 10^5 cells ml^{-1} —the light detector would fail to discretize individual light pulses and a form of ‘pileup’ would occur wherein cell densities were underestimated. To ensure the accuracy of the OCPC approach before the culture reached this density, we compared density measurements done with the OCPC system with those done by manual cell counting (at specific

densities between 10^2 and 3×10^4 cells ml^{-1}) to form a comparative standard curve. From this, we obtained an expected linear relationship, showing agreement between the measurement methods.

We ran the OCPC experiment separately with eleven cultures in 10 ml volumes in cut test-tubes starting with densities of 10^2 cells ml^{-1} in syringe-filtered HL5. From these runs, we subtracted the spectrum obtained by running a culture media without cells. The combined subtracted spectra, compiled using a custom code in *R*, provided our high precision proliferation time series results given in figure 1(f).

4.6. Variable stir rate experiments

To examine the possible relationship between cell proliferation rates and cell collision rates, we employed the turbidity point measurement method (figure 7,

section 4.4) again, but varied the stir rate. The relationship used between collision rate and stir rate is detailed in reference [15]. We ran this experiment three times with 77 vials, stirring them at 16 rpm, 32 rpm, and 64 rpm. We estimate the Reynolds number (Re), the ratio of inertial to viscous forces [31] from the expression $Re = L \frac{U}{\nu}$ where L is the characteristic length which we take to be 0.6 mm, half the depth of the fluid in the vial, U is the characteristic fluid velocity which we take to be the vial radius (0.5 cm) times the angular rotation speed and ν is the kinetic viscosity of the system, which we take to be that of water. In this manner, we established that we were using Re in the range of from 5 to 20, and hence is well described as viscosity dominated flow [31]. This is in contrast to our 150 rpm orbital shaker system (section 4.2) where we expect the characteristic length to be several cm and hence at least two orders of magnitude higher in Re , thereby introducing unstable flow (p 25 of reference [31]). In summary by relying on viscous flow our rotating vial system provides proper control of the shear rate and therefore also the cell–cell collision rate, as required.

4.7. Conditioned media experiments

Unlike in our original experiments [15], detailed in SI section 5, where we used syringe filtering to remove cells, our present work made use of centrifugation. We verified by counting that cells had been removed down to a level of 40–80 cells ml^{-1} . Because of this uncertainty, we started with initial densities of 500 cells ml^{-1} .

With attention to conditioning the media for long periods of time we prepared CM from cells at three different densities: 2×10^3 cells ml^{-1} (below the slow-to-fast transition), 3×10^5 cells ml^{-1} , and 5×10^5 cells ml^{-1} (both above the slow-to-fast transition). The cells at 2×10^3 cells ml^{-1} density were obtained by culturing a 10^3 cells ml^{-1} sample in a fresh HL5 medium for 22 h. We obtained the latter 3×10^5 cells ml^{-1} and 5×10^5 cells ml^{-1} cultures by starting a cell culture at 10^4 cells ml^{-1} and growing them for 72 h. As always we grew samples on a 150 rpm orbital shaker.

4.8. Cluster decay rate measurements

To examine the rates of cluster decay, we transferred samples from suspension cultures onto Petri dishes with cover slip substrates (Part No. P50G-1.5-14-E, MatTek Corporation, Ashland, MA)—covered with mineral oil or hermetically sealed to prevent evaporation. We then observed with digital video as in references [19, 25] over hours with an inverted microscope using an ImageJ digital vision program. Cells shedding from clusters were scored from time series by eye watching recordings in order to estimate the decay rate. In applying this estimate of cluster decay

rate in suspension culture, we are making two approximations: the observations were on surfaces, not in suspension and the attraction of cells for the hydrophilic substrate that might lead to enhanced declustering (note figure 4 of reference [15]) was not considered.

Acknowledgments

We gratefully acknowledge Stephen H Zinder and Susan Merkel of the Department of Microbiology at Cornell University for their advice and aid with bacterial contamination tests. We are indebted to Marek Dolleiser at Sydney University for generously providing the PRA program and his helpful advice. This work was supported by the Cornell Center for Materials Research (MRSEC) (DMR-1719875) with funding from the Research Experience for Undergraduates program (Zhou, Xiao-Qiao, NSF DMR REU Site Grant 0552782 for 2009, Strandburg-Peshkin, Ariana; and Rappazzo, Brendan NSF MRSEC Grant). We also benefitted from the use of their central facilities. We are grateful to the Dicty Stock Center at Northwestern University for providing strains and especially to Petra Fey and Kerry Shepherd for advice [32]. We deeply appreciate the assistance provided by Xiaoning Wang, Benjamin Yavitt, Anthony Hazel and Junseok Oh. Zijin Huang provided valuable background information, alternative analysis and editing. We also appreciate the comments of Robert Insall, University of Glasgow. We are indebted to Eberhard Bodenschatz for providing instruments and advice. Finally, we are in debt to our referees for their vital comments.

Data availability statement

Data and codes that support the findings of this study are available at <https://github.com/carlfranck/Allee-Effect-Physical-Biology-January-2022> [33].

ORCID iDs


Igor Segota  <https://orcid.org/0000-0001-8168-6144>

Matthew M Edwards  <https://orcid.org/0000-0001-9134-4666>

Arthur Campello  <https://orcid.org/0000-0003-0178-7709>

Brendan H Rappazzo  <https://orcid.org/0000-0003-3417-2372>

Xiaoning Wang  <https://orcid.org/0000-0002-2411-7399>

Ariana Strandburg-Peshkin  <https://orcid.org/0000-0003-2985-6788>

Xiao-Qiao Zhou  <https://orcid.org/0000-0002-0724-5153>

Archana Rachakonda  <https://orcid.org/0000-0002-2861-1159>

Kayvon Daie  <https://orcid.org/0000-0003-4584-8227>

Alexander Lussenhop  <https://orcid.org/0000-0002-4044-0401>

Sungsu Lee  <https://orcid.org/0000-0003-3683-7630>

Kevin Tharratt  <https://orcid.org/0000-0002-4711-9856>

Amrish Deshmukh  <https://orcid.org/0000-0002-2733-2844>

Elisabeth M Sebesta  <https://orcid.org/0000-0002-0563-7348>

Myron Zhang  <https://orcid.org/0000-0002-0767-3844>

Sharon Lau  <https://orcid.org/0000-0001-6162-9687>

Sarah Bennedsen  <https://orcid.org/0000-0001-6127-2227>

Jared Ginsberg  <https://orcid.org/0000-0002-0071-2169>

Timothy Campbell  <https://orcid.org/0000-0002-7376-5608>

Chenzheng Wang  <https://orcid.org/0000-0002-4419-4527>

Carl Franck  <https://orcid.org/0000-0002-5036-0894>

References

- [1] Allee W C 1931 *Animal Aggregations. A Study in General Sociology* (Chicago, IL: University of Chicago Press)
- [2] Courchamp F, Berec L and Gascoigne J 2008 *Allee Effects in Ecology and Conservation* (New York: Oxford University Press)
- [3] Drake J M and Kramer A M 2011 Allee effects *Nat. Educ. Knowl.* **3** 2
- [4] Stephens P A and Sutherland W J 1999 Consequences of the Allee effect for behaviour, ecology and conservation *Trends Ecol. Evol.* **14** 401
- [5] Taylor C M, Davis H G, Civile J C, Grevstad F S and Hastings A 2004 Consequences of an Allee effect in the invasion of a pacific estuary by *Spartina alterniflora* *Ecology* **85** 3254
- [6] Aulino P et al 2010 Molecular, cellular and physiological characterization of the cancer cachexia-inducing C26 colon carcinoma in mouse *BMC Cancer* **10** 363
- [7] Casciato D A 2009 *Manual of Clinical Oncology* 6th edn (Philadelphia, PA: Williams & Wilkins)
- [8] Rotem E, Loinger A, Ronin I, Levin-Reisman I, Gabay C, Shores N, Biham O and Balaban N Q 2010 Regulation of phenotypic variability by a threshold-based mechanism underlies bacterial persistence *Proc. Natl. Acad. Sci. USA* **107** 12541
- [9] Christensen S T, Leick V, Rasmussen L and Wheatley D N 1997 Signaling in unicellular eukaryotes *Int. Rev. Cytol.* **177** 181
- [10] Tanabe H, Nishi N, Takagi Y, Fumio W, Akamatsu I and Kaji K 1990 Purification and identification of a growth factor produced by *Paramecium tetraurelia* *Biochem. Biophys. Res. Commun.* **170** 786
- [11] Whitbread J A, Sims M and Katz E R 1991 Evidence for the presence of a growth factor in *Dictyostelium discoideum* *Dev. Genet.* **12** 78
- [12] Pommerville J 2010 *Alcama's Fundamentals of Microbiology* (Boston: Jones and Bartlett)
- [13] Greig D and Travisano M 2004 The prisoner's dilemma and polymorphism in yeast SUC genes *Proc. Biol. Sci.* **271** S25
- [14] Fey P, Kowal A S, Gaudet P, Pilcher K E and Chisholm R L 2007 Protocols for growth and development of *Dictyostelium discoideum* *Nat. Protoc.* **2** 1307–16
- [15] Franck C, Ip W, Bae A, Franck N, Bogart E and Le T T 2008 Contact-mediated cell-assisted cell proliferation in a model eukaryotic single-cell organism: an explanation for the lag phase in shaken cell culture *Phys. Rev. E* **77** 041905
- [16] By optimizing the coefficient of determination (R^2) with a fitting function composed of two straight lines as in https://en.wikipedia.org/wiki/Coefficient_of_determination. The uncertainties in the y values were given by the normal standard errors as in <https://3.nd.edu/~rwilliam/stats1/x91.pdf>
- [17] Lauffenburger D A and Linderman J J 1993 *Receptors: Models for Binding, Trafficking and Signaling* (New York: Oxford University Press)
- [18] In our original manuscript submission, there was a second run included in figure 1(a) that was comprised of five simultaneously-measured specimens vs the six shown in the current version of figure 1(a). In reviewing our lab journal while preparing the revised manuscript we came to suspect that the shaker had been accidentally turned off for a day in the middle of the run. For this reason, we chose to not include the data in figure 1(a) and the analysis presented in table 1. Nevertheless, the behavior of the second data set is indistinguishable by eye from that of the first. The experimental data in figure 5(b) is in fact the average of all original 11 runs. In view of the wide variation in the slow–fast transition show in table 1, a main point of this paper, we regard any correction to figure 5(b) as insignificant.
- [19] Segota I, Mong S, Neidich E, Rachakonda A, Lussenhop C J and Franck C 2013 High fidelity information processing in folic acid chemotaxis of *Dictyostelium amoebae* *J. R. Soc. Interface* **10** 20130606
- [20] Bozzaro S 2006 Assaying cell–cell adhesion *Methods in Molecular Biology (Dictyostelium discoideum Protocols)* vol 146 *Dictyostelium discoideum* L Eichinger and F Rivero (Totowa, NJ: Humana Press) p 449
- [21] Probstein R F 1994 *Physicochemical Hydrodynamics* (New York: Wiley-Interscience) p 248
- [22] Kessin R H 2001 *Dictyostelium: Evolution, Cell Biology and the Development of Multicellularity* (Cambridge: Cambridge University Press)
- [23] Conversation.
- [24] Nowak M A 2006 *Evolutionary Dynamics: Exploring the Equations of Life* (Cambridge, MA: Harvard University Press) p 46
- [25] Segota I, Boulet L, Franck D and Franck C 2014 Spontaneous emergence of large-scale cell cycle synchronization in amoeba colonies *Phys. Biol.* **11** 036001
- [26] Fey P, Kowal A S, Gaudet P, Pilcher K E and Chisholm R L 2007 Protocols for growth and development of *Dictyostelium discoideum* *Nat. Protocols* **2** 1307
- [27] Bastounis E, Meili R, Alonso-Latorre B, del Álamo J C, Lasheras J C and Firtel R A 2011 The Scar/WAVE complex is necessary for proper regulation of traction stresses during amoeboid motility *Mol. Biol. Cell* **22** 3995
- [28] Tsevetkov D, Kolpakov E, Kassmann M, Schubert R and Gollasch M 2019 Distinguishing between biological and technical replicates in hypertension research on isolated arteries *Front. Med.* **6** 126
- [29] Dolleiser M PRA Version 8 <https://www.gammaspectacular.com/psectacular.com/marek/pr/index.html>
- [30] Many design iterations of the stir system were tested before one was found that did not exhibit apparent shedding of the stirbar's Teflon coating. We also discovered that drying sterilized sample cells with a compressed gas duster could

- introduce a significant number of extraneous particles into the chamber.
- [31] Tritton D J 1991 *Physical Fluid Dynamics* (Oxford: Oxford University Press) p 14
- [32] Fey P, Dodson R J, Basu S and Chisholm R L 2013 One stop shop for everything Dictyostelium: dictyBase and the Dicty Stock Center in 2012 *Dictyostelium discoideum Protocols (Methods in Molecular Biology)* vol 983 (Totowa, NJ: Humana Press) ed L Eichinger and F Rivero pp 59–92
- [33] <https://github.com/carlfranck/Allee-Effect-Physical-Biology-January-2022>